Integrated Positioning for Connected Vehicles

Anas Mahmoud, Aboelmagd Noureldin, *Senior Member, IEEE*, and Hossam S. Hassanein, *Fellow, IEEE*

***Abstract*— In the era of autonomous cars, accurate vehicular positioning becomes very essential. The global navigation satellite systems (GNSS) suffer from signal blockage and severe multipath in urban canyons, which degrades the positioning accuracy and availability. Therefore, vehicles solely relying on positioning from GNSS receivers have limited performance. In this research, we present a novel unified cooperative positioning solution which enhances positioning accuracy and availability in urban canyons. The proposed system exploits the fact that vehicles have different positioning resources and is based on angle approximation, which artificially generates the hindered pseudorange by sharing angle information between vehicles using dedicated short-range communication. In addition, we propose a system that employs the proposed cooperative technique to assist the loose integration between the inertial navigation system (INS) and the GPS system (using extended Kalman filter) during partial GPS outages. Using raw data from inertial sensors and GPS receivers in the real road trajectories, we implement the cooperative INS/GPS loose integration and show that our cooperative integrated system outperforms the non-cooperative integrated system. The performance metrics used are the 2-D positioning root-mean-square error, the maximum 2-D positioning error, and the positioning accuracy gain (PAG). Specifically, the PAG gain is around 88%, 80%, and 60% when the number of blocked satellites is one, two, and three, respectively.**

***Index Terms*— Cooperative positioning, connected vehicles, urban areas.**

I. Introduction

INTELLIGENT Transportation Systems (ITS) aim at reducing traffic accidents and congestion. In addition, ITS systems enable many applications including entertainment and driver assistance applications. The recent developments in Vehicular Ad-Hoc Networks (VANETs) and Dedicated Short Range Communication (DSRC) enabled many of the ITS applications. Information about the position of the vehicles are used by many ITS applications and Location-Based Services (LBS). For example, in automated driving modes and safety critical applications, vehicles have to exchange their accurate positions. The required positioning accuracy and availability of the vehicles' position depends on the application.

Manuscript received December 11, 2017; revised July 1, 2018 and December 10, 2018; accepted December 19, 2018. Date of publication February 11, 2019; date of current version December 31, 2019. This work was supported by the Natural Sciences and Engineering Research Council of Canada under Grant STPGP 479248. The Associate Editor for this paper was K. Wang. *(Corresponding author: Anas Mahmoud.)*

A. Mahmoud was with the School of Computing, Queen's University, Kingston, ON K7L 3N6, Canada. He is now with the MEMS Sensor Group, TDK Invensense, Calgary, AB T3B 4M1, Canada (e-mail: anass.samir@gmail.com).

A. Noureldin is with the Department of Electrical and Computer Engineering, Royal Military College of Canada, Kingston, ON K7K 7B4, Canada.

H. S. Hassanein is with the School of Computing, Queen's University, Kingston, ON K7L 3N6, Canada.

Digital Object Identifier 10.1109/TITS.2019.2894522

In urban environments, the positioning accuracy and availability of land vehicles is limited. Tall buildings block signals from various Global Navigation Satellite Systems (GNSS). In addition, buildings and other objects in dense urban areas also reflect GNSS signals causing severe multipath effects. Moreover, vehicles in urban areas have different positioning capabilities:

- A limited number of vehicles are capable of decoding multi-constellation GNSS signals.
- A limited number of vehicles employ advanced multipath detection and mitigation techniques.
- A limited number of vehicles employ advanced anti-jamming (e.g., using multiple antennas) detection and mitigation techniques.

Accurate positioning of vehicles is required by most safety critical ITS applications. Positioning systems can be categorized as non-cooperative (conventional) and cooperative systems. Due to the harsh signal environment in urban areas, non-cooperative systems suffer from limited positioning accuracy [1]. Recently, Cooperative Positioning (CP) has been proposed as an ideal solution to the problem of limited positioning accuracy in urban environments. CP takes advantage of the fact that vehicles have different positioning resources and uses DSRC to exchange positioning information between vehicles and subsequently estimate accurate positions. Most of the proposed systems rely on ranging methods to estimate the distance between vehicles or between vehicles and Road-Side-Units (RSUs). Ranging methods introduce range errors to the estimated distances [2]. These errors propagate to the final computed position and thus, the performance of the range based CP systems are also limited.

This paper aims at introducing a CP system that utilizes the exchange of pseudoranges from assisting vehicles to aid INS/GPS Loosely Coupled integration using Extended Kalman Filter (LC-EKF). The proposed system enhances the performance of the LC-EKF during partial GPS outages. The Reduced Inertial Sensor System (RISS) mechanization process is utilized in this research. Both the system and measurement model of the LC-EKF which are presented in this research are used to fuse the INS and the GPS states. We conduct real experiments by collecting road trajectories in Kingston, Ontario. The proposed system is compared to the existing LC-EKF during all simulated GPS partial outages to exmaine its performance.

II. Background and Literature Review

There are two main approaches used to enhance positioning of vehicles. Non-cooperative and CP positioning approaches.

This research focuses on positioning of vehicles in very challenging environments like urban areas where most of the conventional positioning techniques fail to meet the requirements of ITS applications. Here, we will only provide a literature review of the most common cooperative positioning techniques in the literature. Moreover, we will introduce the advantages of INS/GPS integration.

A. Cooperative Positioning

Extensive research has been conducted in the area of Wireless Sensor Network (WSN) localization. Many of the proposed methods rely on CP techniques to enhance the positioning accuracy of the nodes. Some of the WSN positioning methods have been re-proposed in the domain of VANETs. However, the main difference between WSN and VANETs is the high mobility of the nodes in the network. Moreover, WSN nodes have very limited processing capabilities compared to nodes in VANETs. Some CP methods rely either on the availability of ranging information to other vehicles using Vehicle-to-Vehicle (V2V) communication or the availability of ranging information to RSUs using Vehicle-to-Infrastructure (V2I). Other CP methods do not use ranging techniques due to their limited performance.

1) Ranging-Based Techniques: In order to enhance the position of a vehicle, ranging methods are proposed to estimate the distance between the vehicle to be localized and a reference point with known position. This reference can be a RSU, an adjacent vehicle or a cellular tower. There are two main techniques used to estimate the range between a vehicle and another reference:

- Signal Strength-Based Ranging
- Time-Based Ranging

2) Signal Strength-Based Ranging: The concept behind Received Signal Strength(RSS) based ranging is that the strength of an RF signal decays as the signal propagates. Some research has been directed towards RSS-based ranging in cellular networks [3]. However, the achieved accuracy is in the range of hundreds of meters and therefore is not suitable for CP. Other research directions in the field of WSN localization [4]–[6], assume that α is the same for all links and is non-changing over time and thus not suitable for VANETs dynamic environment where many obstacles exist.

The work in [7] and [8], attempts to enhance the positioning accuracy of vehicles in urban areas where multipath is a dominant source of error. Once a vehicle detects a multipath, it requests positions and relative distance from vehicles in its vicinity using CP. An optimization problem is then formulated incorporating information from the participating vehicles with accurate positions and their distances to the target vehicle. The distances are computed using RSS which result in significant relative distance errors.

3) Time-Based Ranging: The first type of Time-Based ranging is Time of Arrival (TOA). In order to estimate the distance between receivers A and B, receiver A sends a packet with a time stamp denoted by T_A which represents the transmission time to receiver B. Receiver B receives the packet and adds another time stamp denoted by T_B which represents the reception time at receiver B. Subsequently, receiver B sends the packet to receiver A. The difference between the reception time and the transmission time multiplied by the speed of light is the distance between receivers A and B. To achieve a meter level accuracy, the clock synchronization between receiver A and B has to be in terms of nanoseconds. In vehicular communications, DSRC uses IEEE802.11p which is based on IEEE802.11. The clock synchronization in IEEE802.11 protocols is in terms of microseconds [9]. This means that the error in the calculated distance will be in terms of thousands of meters.

Another Time-based ranging technique is Time Difference Of Arrival (TDOA). In this ranging method, two signals from two stations are transmitted and the vehicle to be localized processes the difference between the arrival time of both signals to identify the locus of the vehicle [10]. The most important constraint is that the two stations have to be synchronized to the nanosecond level. Vehicles using DSRC can not reach such level of synchronization. TOA and TDOA require very complex hardware to achieve the time synchronization between vehicles and therefore both methods are not practical for determining ranges between vehicles in VANETs.

A third Time-Based ranging approach is Round Time Trip (RTT) and is the most promising technique in terms of ranging accuracy. The distance is computed using the round time trip of the signal between two vehicles. Synchronization is not required between the two vehicles because the relative distance is computed relative to one clock. However, the processing and the queuing time need to be modeled in order to estimate the correct relative distance.

In [11], a localization framework for VANETs is proposed. Using TOA as a ranging method, the distance between vehicles is estimated. Moreover, a particle filter is used to fuse GNSS position, odometer reading and distance between vehicles to enhance the position of vehicles. A map matching algorithm is used to enhance the vehicle's position. The author assumes that the error in the estimated distance due to mis-synchronization between the receivers is in terms of tens of meters which should reflect a mis-synchronization in terms of nanoseconds. This is not a realistic assumption and hence the results are not practical. Moreover, in urban areas, multipath signals are dominant due to many reflectors and thus degrades the performance of TOA and TDOA. References [12]–[15] present different TOA and TDOA ranging approaches. Due to their synchronization requirements, these approaches are not practical for VANET positioning and will not be discussed further.

4) Non Ranging-Based Techniques: Range-Based techniques suffer from many limitations that prevent the usage of such techniques in CP. A detailed discussion of the limitations of the ranging-based techniques is presented in [2]. Non Range-Based techniques do not rely on time or signal strength ranging techniques. References [16] and [17] assume no GNSS coverage is available and propose a method by which vehicles can estimate their positions and also their lane. Two RSUs on the opposite sides of the road broadcast their position and road geometry information. Using the broadcasted information, the odometer measurements and the

Carrier-Frequency-Offset (CFO) of the received signals from the RSUs, vehicles compute their position and lane. This approach is very expensive since it requires RSUs storing information about the road geometry to be installed at each intersection.

Using only two GNSS satellites, vehicle to infrastructure communication and RSS of the DSRC packets, Alam [18] proposes a CP positioning method. This method is based on intersecting the equation of the line representing the street with the TDOA hyperboloid from the two GNSS satellites to estimate the vehicles position. A Doppler shift filter is used to mitigate multipath. This method assumes an RSU is installed at each intersection and broadcasts its positions. Hence, it is an expensive solution. The filter used to mitigate multipath is based on observing Doppler shifts from the RSUs. However, for low vehicle speeds, Doppler shifts are not observed due to the high noise threshold [18].

In [19], pseudorange measurements are exchanged between two vehicles. Using Double Differencing (DD) and a tightly coupled particle filter is used to estimate the relative distance between vehicles. The concept of DD is close to DGPS since the common errors are removed from the pseudoranges of both vehicles. The real time response of the particle filter is questionable and the proposed method assumes full satellite coverage which is not suitable for VANETs in dense urban areas.

In [21], a system is proposed for estimating the relative distance between vehicles in urban areas when the number of visible satellites is at least four. Pseudoranges are exchanged between vehicles and a form of DD is applied to remove the common errors. A tight integration is adopted fusing the DD values to estimate the relative distance between vehicles. Even though, the proposed system eliminates the need for a DGPS infrastructure, it does not mention multipath. Multipath is dominant in dense urban areas and will certainly degrade the performance of the proposed system. In [20], a system is proposed for enhancing the position of vehicles in urban areas when the number of visible satellites is at least four. Loose integration is adopted for fusing GPS position with range-rate estimated from the CFO of the received signals from adjacent vehicles. The range-rate estimation is based on observing Doppler shifts. In order to be able to observe the Doppler shifts, a minimum relative speed between vehicles should exist. In urban areas, the relative speeds between vehicles are very low and hence the proposed system is not effective.

B. INS/GPS Integration

The solution estimated using a GPS receiver has different characteristics compared to the solution estimated by an INS system. Due to the complementary characteristics of the GPS and INS systems, integrating both systems has been extensively used in practice. Table I summarizes the characteristic of the solution offered by the commercial GPS receiver and an INS system. GPS solution can be used to aid INS by slowing down the accumulation of error. On the other hand, INS systems can extrapolate solutions by estimating states during short GPS outages. Finally, using an INS and GPS integrated solution provides an accurate position, velocity and attitude information. It is worth noting that the accuracy of the estimated states depends on the grade of the INS (whether strategic or MEMS-based) and the complexity of the GPS receiver.

TABLE I
SUMMARY OF GPS AND INS IMPORTANT FEATURES

Features	GPS	INS
Positioning Type	Absolute Positioning	Relative Positioning
Accuracy	Good in long-term	Good in short-term
Attitude	Not Available	Available
Sensitive to Jamming	Yes	No
Sensitive to Gravity	No	Yes
Sampling Rate	Low	High
Functions Indoor	No	Yes

III. METHODOLOGY

A. Proposed Cooperative System

In an urban environment, vehicles are equipped with different positioning resources. Some expensive vehicles are capable of decoding many GNSS constellations while others might only track GPS satellites. Different vehicles employ INS systems that vary in grades. Some vehicles use advanced signal processing techniques to detect and mitigate jamming and short delayed multipath signals while other vehicles are only capable of detecting and mitigating medium and long delayed multipath signals and might not have the necessary hardware resources (array of antennas) to mitigate the effect of jamming signals. The need for utilizing resources from neighboring vehicles in a cooperative manner to assist in enhancing the positioning availability and accuracy of other vehicles is critical in dense urban areas.

In this paper, a cooperative positioing system based on [23] is presented. We design a system that utilizes DSRC transceivers to request pseudoranges from vehicles within the communication range of a target vehicle. Using Angle Approximation (AA), a vehicle selection method (ASOSD) and a satellite selection method (ASODD), we artificially reconstruct the hindered pseudoranges of the target vehicle and hence enhance the performance of the INS/GPS filter during partial GPS outages. In order to design a navigation system which is commercially viable and affordable, MEMS-based sensors are used in vehicular navigation. The errors of MEMS-based sensors are very complex and thus can be used in standalone mode only for very short durations. On the other hand, GPS errors are bounded but the visibility of at least four satellites is essential for estimating a 3D position and velocity. The implementation of the LC filter is very simple, however, its main drawback is the low positioning accuracy when GPS outages are prolonged. This is due to the fact that only INS solution is used when the number of visible satellites is less than four.

Figure 1 depicts the proposed cooperative RISS/GPS LC-EKF (CLC-EKF) system which consists of three main components. We assume that a target vehicle v_j is not capable of estimating pseudoranges to at least 4 satellites. The first

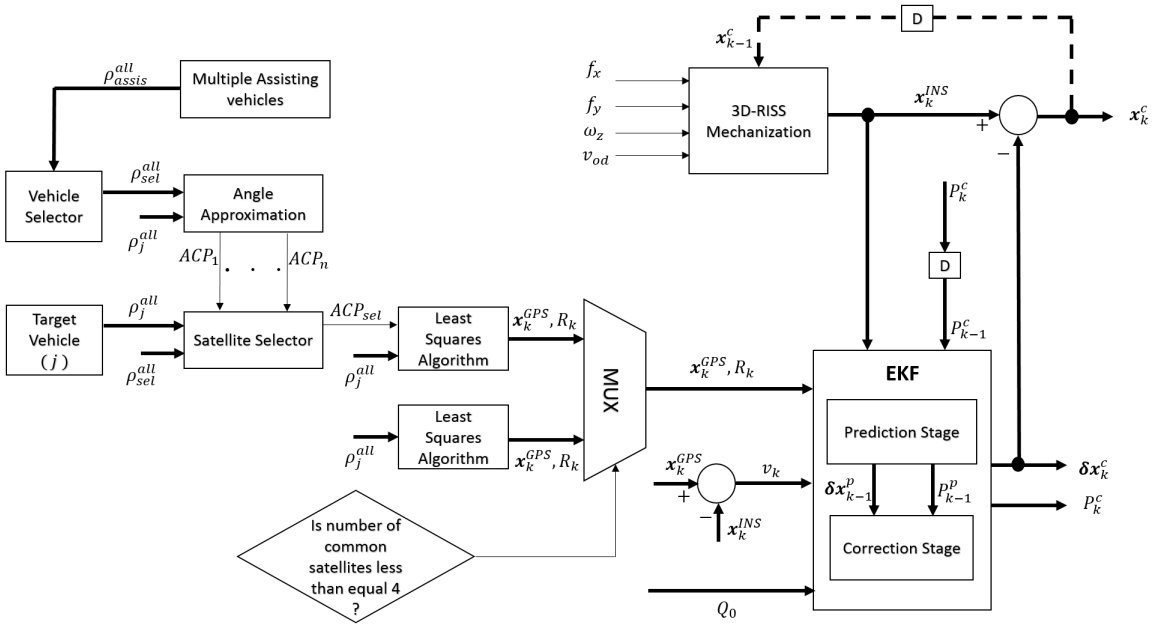

Fig. 1. Proposed cooperative 3d-riss/gps lc-ekf system.

block in the proposed system depicts the Angle Approximation technique which aids in reconstructing the missing pseudoranges of v_j. The first block also includes an assisting vehicle selector which decides which assisting vehicle to rely on in order to reconstruct v_j pseudoranges. Moreover, a satellite selector is utilized to determine which satellite to rely on in order to reconstruct v_j pseudoranges.

The second component is the 3D Reduced Inertial Sensor System (RISS) mechanization process used to estimate the states of v_j. In addition, the last component of our proposed system is using LC Extended Kalman Filter (LC-EKF) for the fusion of the RISS and the GPS solution to estimate an optimal position. When the number of visible satellites to v_j is at least four, a least squares algorithm is applied to the measured pseudoranges. However, if the number of visible satellites is less than four, the reconstructed pseudoranges are used to estimate the GPS position.

B. Blocked Pseudorange Estimation

In this Section, we introduce the concept of Angle Approximation (AA). In addition, the Absolute Sum of Double Differencing (ASODD) method for satellite selection and the Sum of Single Differencing (ASOSD) method for vehicle selection are briefly presented.

1) Angle Approximation: In [24], we propose a geometric method by which a target vehicle v_j relies on assisting vehicles to estimate a blocked pseudorange. This method is called Angle Approximation (AA). Assume pseudoranges from satellites k, m and n are available to vehicles v_i and v_j, while the pseudorange from satellite f is only available to v_i. Figure 2 depicts only satellites k and f. This occurs in urban canyons due to the existence of obstacles. Moreover, Blockage even for small distances between vehicles can also occur when the receiver of the target vehicle has the capability of only

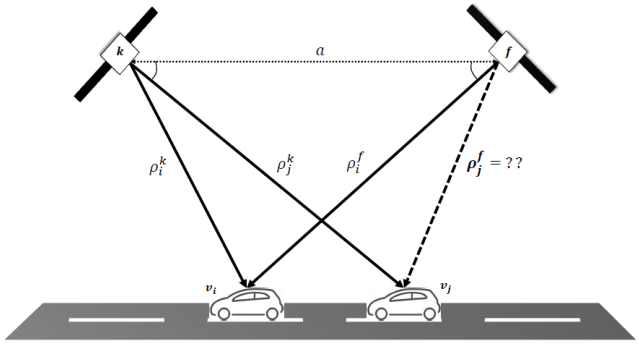

Fig. 2. Angle approximation for ACP generation.

decoding GPS signals, while the receiver of the assisting vehicle is capable of decoding both GPS and GLONASS signals. Furthermore, v_j might have the capability of decoding GPS/GLONASS but a jamming signal could lead to the blockage of GLONASS constellation, while v_i uses complex anti-jamming algorithms. Therefore, v_i has access to more satellites than v_j. Hence, v_j is either not capable of computing a 3D position due to the limited number of equations compared to the number of unknown states or is capable of computing a position with poor accuracy.

The distances between the satellites and the vehicles are significantly larger than the distance between the vehicles, pseudoranges ρ_i^k, ρ_j^k and also ρ_i^f, ρ_j^f are almost parallel [22]. Therefore, we can conclude that the angle between pseudoranges ρ_i^k and ρ_i^f denoted by $\theta_i^{k,f}$ in Figure 2 is almost equal to the angle between pseudoranges ρ_j^k and ρ_j^f denoted by $\theta_j^{k,f}$. The following steps demonstrate how ρ_j^f is generated using AA:

1) v_j receives periodic beacons containing visible satellites from v_i using DSRC and detects that the signal from satellite f is blocked or jammed.
2) v_j is ready to execute the AA technique. First the angle $\theta_i^{k,f}$ is computed using the cosine rule in (1)
3) Under the assumption $\theta_i^{k,f} \cong \theta_j^{k,f}$, vehicle j generates pseudorange ρ_j^f by solving quadratic equation (2). Denote by $\rho_j^{f,k}$ the generated pseudorange using ρ_i^k. Here, $\rho_j^{f,k}$ is called an Artificial Candidate Pseudorange ACP) for the hindered pseudorange ρ_j^f.

$$\theta_i^{k,f} = \cos^{-1} \frac{(\rho_i^k)^2 + (\rho_i^f)^2 - (a)^2}{2\rho_i^k \rho_i^f} \tag{1}$$

$$(\rho_j^{f,k})^2 - 2\rho_j^k \rho_j^{f,k} \cos\theta_i^{k,f} + ((\rho_j^k)^2 - a^2) \cong 0 \tag{2}$$

In the previous example, the number of common satellites between vehicle i and j is three. Therefore, the AA technique can be executed several times using three angle approximations resulting in three different ACPs for the hindered pseudorange. Assuming $\theta_i^{k,f} \cong \theta_j^{k,f}$, AA generates the hindered pseudorange using satellite k, such that $\rho_j^{f,k}$ is expressed by 3. Here, $\mu^{f,k}$ denotes the error due to the inaccuracy of the $\theta_i^{k,f} \cong \theta_j^{k,f}$ assumption.

$$\rho_j^{f,k} = \rho_j^f + \mu^{f,k} \tag{3}$$

Similarly, assuming $\theta_i^{m,f} \cong \theta_j^{m,f}$ and $\theta_i^{n,f} \cong \theta_j^{n,f}$ respectively generate $\rho_j^{f,m}$ and $\rho_j^{f,n}$. Now the most critical question becomes: which ACP should the receiver use to compute its position. In [24], we discuss several factors affecting the accuracy of the ACP including distance between the target and assisting vehicle and geometry of the common and non-common satellites. The ultimate goal is to use the ACP which is based on the most accurate angle approximation since it would result in the least range error.

2) Satellite Selection: In order to infer which aritfically candidate pseudorange is the most accurate, we propose a satellite selector called Absolute Sum of Double Differencing (ASODD). The ASODD selector uses the measured pseudoranges from v_i and v_j and all the corresponding ACPs representing the blocked pseudorange to compute a positive indicator for the correctness of each ACP.

Following the AA assumption, the angle between the two pseudoranges from satellites k and f to v_i is approximately equal to the angle between the two pseudoranges from satellites k and f to v_j. Hence, the double differencing of the pseudoranges k and f from vehicle i and j tends to zero. The idea behind ASODD is to apply a sequence of mathematical operations to the ACPs which leads to the accumulation of the error due to AA. The absolute value of the sum of the double differencing of the pseudoranges indicates how far each generated ACP is from meeting the angle approximation assumption.

Assume satellites k, m and n are visible to the participating vehicle i and the target vehicle j. While satellite f is only visible to vehicle i. Using the assumptions $\theta_i^{k,f} \cong \theta_j^{k,f}$, $\theta_i^{m,f} \cong \theta_j^{m,f}$ and $\theta_i^{n,f} \cong \theta_j^{n,f}$, the AA technique generates three pseudoranges $\rho_j^{f,k}$, $\rho_j^{f,m}$and $\rho_j^{f,n}$ with errors $\mu^{f,k}$, $\mu^{f,m}$ and $\mu^{f,n}$ respectively. Here we will derive the ASODD indicator for $\rho_j^{f,k}$ in details. Equation 4 depict the actual pseudorange.

$$\rho_j^f = R_j^f + \beta_j + \alpha^f + \varepsilon_j^f \tag{4}$$

where

- R_j^f is the true range from vehicle j to satellite f.
- β_j is the clock bias of vehicle j and the receiver's noise (common errors to a single receiver).
- α^f is the clock bias of satellite f, the ionosphere and troposphere errors(common errors to a single satellite).
- ε_j^f is the error due to multipath.

Our main aim is to attenuate the value ρ_j^f in (3) and amplify the generated error denoted by $\mu^{f,k}$, such that the error in the candidate pseudorange is observable.

Denote by $ASODD^{f,k}$ the ASODD indicator for the ACP $\rho_j^{f,k}$. This quantity is calculated by taking the sum of the absolute value of the double differencing between the ACP and all the other observable pseudoranges from vehicles i and j. $ASODD^{f,k}$ is given by

$$ASODD^{f,k} = \sum_{s=k,m,n} |\Delta\rho_i^{sf} - \Delta\rho_j^{sf,k}| \tag{5}$$

where s is the number of common visible satellites between v_i and v_j

$$ASODD^{f,k} = |\Delta\rho_i^{kf} - \Delta\rho_j^{kf,k}| + |\Delta\rho_i^{mf} - \Delta\rho_j^{mf,k}| + |\Delta\rho_i^{mf} - \Delta\rho_j^{mf,k}| \tag{6}$$

$\Delta\rho_i^{kf}$ is the difference between the pseudorange ρ_i^k and ρ_i^f. This difference eliminates the clock bias of vehicle i and the receiver's noise. Similarly, $\Delta\rho_j^{mf,k}$ and $\Delta\rho_j^{nf,k}$ is the difference between ρ_j^m and $\rho_j^{f,k}$ and ρ_j^n and $\rho_j^{f,k}$ respectively. This step removes the receiver's clock bias and noise from all the pseudoranges of vehicle j. The effect of the second step of the double differencing is removing the satellite's clock bias.

Likewise, the absolute double differencing in the ASODD indicator;$|\Delta\rho_i^{mf} - \Delta\rho_j^{mf,k}|$ and $|\Delta\rho_i^{nf} - \Delta\rho_j^{nf,k}|$ can be calculated. Therefore, (6) can be represented as:

$$ASODD^{f,k} = |\Delta R_{ij}^{kf} + \Delta\varepsilon_{ij}^{kf} + \mu^{f,k}| + |\Delta R_{ij}^{mf} + \Delta\varepsilon_{ij}^{mf} + \mu^{f,k}| + |\Delta R_{ij}^{nf} + \Delta\varepsilon_{ij}^{nf} + \mu^{f,k}| \tag{7}$$

where:

- ΔR_{ij}^{kf}, ΔR_{ij}^{mf} and ΔR_{ij}^{nf} are the double differencing terms for the difference in the true ranges.
- $\Delta\varepsilon_{ij}^{kf}$, $\Delta\varepsilon_{ij}^{mf}$ and $\Delta\varepsilon_{ij}^{nf}$ are the double differencing terms for the multipath error. It is not removed because it is not common between the pseudoranges. Here we assume multipath is almost zero because pseudoranges affected by severe multipath are not used to generate hindered

pseudoranges. Therefore, 7 can be approximated by:

$$ASODD^{f,k} = |\Delta R_{ij}^{kf} + \mu^{f,k}| + |\Delta R_{ij}^{mf} + \mu^{f,k}| + |\Delta R_{ij}^{nf} + \mu^{f,k}| \quad (8)$$

Following the same steps, $ASODD^{f,m}$ and $ASODD^{f,n}$ can be derived. Equations 9 and 10 depict the final stage of the derivation.

$$ASODD^{f,m} = |\Delta R_{ij}^{kf} + \mu^{f,m}| + |\Delta R_{ij}^{mf} + \mu^{f,m}| + |\Delta R_{ij}^{nf} + \mu^{f,m}| \quad (9)$$

$$ASODD^{f,n} = |\Delta R_{ij}^{kf} + \mu^{f,n}| + |\Delta R_{ij}^{mf} + \mu^{f,n}| + |\Delta R_{ij}^{nf} + \mu^{f,n}| \quad (10)$$

Equations 8, 9 and 10 consist of the double differencing terms for the true ranges and the error in the generated pseudoranges. The error in the generated pseudoranges accumulates several times for each indicator depending on the number of common satellites between the target and the assisting vehicle. Consequently, ASODD increases the probability of observing the magnitude of the error for each ACP. Hence, the ASODD indicator can be used to select the least erroneous ACP.

3) Vehicle Selection: In urban areas, several vehicles are within the communication range of the target vehicle. Some of those vehicles can assist the target vehicle in either enhancing positioning availability or accuracy. In [25], we propose a method called Absolute Sum of Single Differencing (ASOSD) by which one assisting vehicle is selected from the candidate assisting vehicles. After a single assisting vehicle is selected, AA is applied to generate ACPs and then ASODD is used to select the final ACP. Here, the final ACP refers to the pseudorange which will be used in the final position estimation.

The accuracy of the AA method is affected by the distance between vehicles. Hence, the distance between the candidate assisting vehicles and the target vehicle is the most important factor affecting the accuracy of the generated ACPs. The ASOSD method uses the difference between the common pseudoranges of the target and the Candidate Assisting Vehicles (CAV) to calculate a distance indicator for each vehicle. This method assumes that each CAV can estimate its GNSS receiver's clock bias and the pseudoranges transmitted to the target vehicle are corrected for the error due to the clock bias. Equation 11 is used to calculate the ASOSD distance indicator for a assisting vehicle i denoted by $ASOSD_i$. Assuming S is the number of common satellites between the target and assisting vehicle.

$$\begin{aligned} ASOSD_i &= \sum_{s=1}^{S} |\rho_j^s - \rho_i^s - Clk_i| \\ &= \sum_{s=1}^{S} |(R_j^s + \beta_j + \alpha^s + \varepsilon_j^s) \\ &\quad - (R_i^s + \beta_i + \alpha^s + \varepsilon_i^s) - Clk_i| \\ &\simeq \sum_{s=1}^{S} |(R_j^s - R_i^s) + \beta_j + \varepsilon_j^s| \end{aligned} \quad (11)$$

Removing the assisting vehicle's clock bias denoted by Clk_i in (11) is very important as it is not common to all assisting vehicles. However, the target's clock bias does not need to be removed since the all ASOSD indicators are referenced to the target vehicle. In other words, the target vehicle's clock bias equally affects the ASOSD indicator for each assisting vehicle. Assuming the assisting vehicle's clock bias is correctly estimated and hence $Clk_i \simeq \beta_i$. Moreover, all common errors between pseudoranges to the same satellites are removed. These commmon errors are due to the uncompensated satellite clock bias, ionospheric and troposheric delays.

The non-common errors between the target vehicle j and the assisting vehicle i is denoted by ε_i^s. Assuming non-common errors like multipath or receiver noise at the assisting vehicles are approaching zero. This occurs for example when assisting vehicles are capable of mitigating short delay multipath signals or are not affected by multipath.

The effects of the target's clock bias denoted by β_j and the non-common errors on the pseudoranges of the target vehicle denoted by ε_j^s does not affect the accuracy of the ASOSD distance indicator because they are common to all assisting vehicles.

Using the ASOSD method reduces the complexity of the overall system. When selecting one assisting vehicle based on the distance indicator, the AA and the ASODD selection method is applied only to one vehicle instead of all the assisting vehicles.

C. The 3D Reduced Inertial Sensor System

A full IMU system consists of 3 gyroscopes monitoring angular rotations across the 3-axis of the vehicle. In addition, 3 accelerometers that measure the specific forces across the 3-axis of the vehicle. The full IMU is the most accurate mechanization process, however it is expensive and of high complexity. The 3D RISS [26], [27] is an attempt to reduce the cost and complexity of a full IMU system. The 3D RISS system proposed in the literature consists of 1 gyroscope perpendicular to the horizontal plane and 2 accelerometers parallel to the horizontal plane (one parallel to the x-axis and the other parallel to the y-axis) along with speed information from the wheel rotation sensor (odometer). The advantages of using the partial IMU (3D RISS) over full IMU are discussed in [26]–[28].

The process by which the RISS system computes the states of the land vehicle from the raw data of the sensors is called mechanization. Denote by f_x and f_y the transversal and forward specific forces from the accelerometers respectively. Moreover, the angular rotation rate from the vertical gyroscope and the speed from the odometer are denoted by ω_z and v_{od} respectively. The system states representing the latitude, longitude and altitude are denoted by φ, λ and h respectively. In addition, the system states representing the East, North and Up velocity are denoted by v^e, v^n and v_u respectively. The first step in the 3D RISS mechanization process is the computation of the attitude angles. The pitch and roll angles are computed using specific forces from the accelerometers and an accurate gravity model. Equations 12 and 13 are used to compute the

pitch and roll angles denoted by p and r. The integration of the speed from the odometer yields the acceleration and is denoted by a_{od}

$$p = sin^{-1}\left(\frac{f_y - a_{od}}{g}\right) \tag{12}$$

$$r = -sin^{-1}\left(\frac{f_x - v_{od}\omega_z}{gcos(p)}\right) \tag{13}$$

The azimuth angle denoted by Az is computed using the previous azimuth angle and the current angular rotation rate. Two effects must be removed from the current ω_z measurement. The stationary effect of Earth's rotation denoted by $\omega^e sin(\varphi_{k-1})$ on the output of the vertical gyroscope is removed. Where, the angular rotation rate of Earth denoted by ω^e is approximately 15 degrees per hour ($7.27 * 10^-5$ radians per second) [29] and φ_{k-1} is the latitude from the previous epoch. Moreover, the non-stationary effect (Coriolis effect) is also compensated. Equation 14 is used to compute Az. The current and previous azimuth angles are denoted by Az_k and Az_{k-1} respectively. Here, R_N is the normal radius of curvature of the Earth's ellipsoid.

$$Az_k = Az_{k-1} - \left(\omega_z - \omega^e sin(\varphi_{k-1}) - \frac{v^e_{k-1} tan(\varphi_{k-1})}{R_N + h_{k-1}}\right) \tag{14}$$

The attitude angles p, r and Az are computed and the next stage of the mechanization is computing the East, North and Up velocities. This is performed by transforming the speed measurements from the body frame to the local frame using the transformation matrix. The current attitude angles are used to compute the transformation matrix. Using Equations 15, 16 and 17, v^e, v^n and v^u is computed.

$$v^e = v_{od} sin(Az) cos(p) \tag{15}$$

$$v^n = v_{od} cos(Az) cos(p) \tag{16}$$

$$v^u = v_{od} sin(p) \tag{17}$$

The final stage of the mechanization process is the computation of the position of the platform. East, North and Up velocities are integrated to respectively compute the latitude, longitude and altitude. Equations 18, 19 and 20 yield states of the system representing its position. The sampling time is denoted by Δt and the Meridian radius of curvature of the Earth's ellipsoid is denoted by R_M. The main reason for the unbounded error of the INS system on the long run is the integration process. This is due to the fact that sensors' biases and drifts propagate to the velocities through the attitude angles, and velocities are then integrated every epoch to compute the position of the vehicle.

$$\varphi_k = \varphi_{k-1} + \frac{v^n_k + v^n_{k-1}}{2(R_N + h)}\Delta t \tag{18}$$

$$\lambda_k = \lambda_{k-1} + \frac{v^e_k + v^e_{k-1}}{2(R_M + h)}\Delta t \tag{19}$$

$$h_k = h_{k-1} + \frac{v^u_k + v^u_{k-1}}{2}\Delta t \tag{20}$$

D. System and Measurement Model for 3D-RISS/GPS LC-EKF

In this section, the system and the measurement model of the 3D-RISS/GPS LC-EKF integration is introduced. The main reference for the system and measurement model is [29] unless stated otherwise.

Since a form of KF is used as a data fusion method, the system and the measurement model have to meet the requirements of KF to converge and hence achieve optimal state estimation.

1) System Model: The discrete-time system model of the 3D-RISS/GPS integration can be expressed using the following equation:

$$\mathbf{x_k} = \phi_{k,k-1}\mathbf{x_{k-1}} + G_{k-1}w_{k-1} \tag{21}$$

where

- $\mathbf{x_k}$ is the current state vector of the system
- $\mathbf{x_{k-1}}$ is the previous state vector of the system
- $\phi_{k,k-1}$ is the discrete-time linear state transition matrix which models the deterministic relation between the previous and the current state vectors. Given the dynamic coefficient matrix F of a continuous system, the linearized state transition matrix is shown in Equation 22. where I is the identity matrix.

$$\phi = (I + F\Delta t) \tag{22}$$

- G_{k-1} is the noise coupling matrix.
- k is the measurement epoch.
- w_{k-1} is the system noise.

Equations 12 to 20 are the RISS mechanization equations. These equations are non-linear and in order to meet the KF linearity requirements, linearization of the RISS mechanization equations is essential. Taylor series expansion is applied to the system equations describing the rate of change of the states. Only the first order terms are considered in the transition matrix. Moreover, very small terms are ignored to reduce the complexity of the system. The process of linearization forces the states of the system to become errors in the states. Therefore, the RISS states of the system are given by vector 23. The error in latitude, longitude and altitude is denoted by $\delta\varphi$, $\delta\lambda$ and δh respectively. East, North and Up velocity errors are denoted by δv^e, δv^n and δv^u respectively. Moreover, δAz, δa_{od} and δb_z denote the error in azimuth, error in acceleration due to wheel rotation sensor measurement and gyroscope bias error respectively.

$$\mathbf{x_k} = [\delta\varphi, \delta\lambda, \delta h, \delta v^e, \delta v^n, \delta v^u, \delta Az, \delta a_{od}, \delta b_z] \tag{23}$$

2) Measurement Model: The discrete-time linear measurement model relating the system states to the error in the measurement is given by:

$$\delta z_k = H\delta\mathbf{x_k} + \eta_k \tag{24}$$

where

- δz_k is the error in the measurement vector.
- H is the design matrix. Here the design matrix is not changing with time.
- η_k is the measurement noise.

In the LC implementation of EKF, the integration is performed on the level of states of the system which makes LC implementation simpler than TC implementation. Here we only use the latitude, longitude and altitude estimated by the GPS to aid the INS system. Velocities can also be used to aid the INS system. The measurement vector is given by:

$$\delta z = \begin{bmatrix} \delta\varphi_{GPS} - \delta\varphi_{INS} \\ \delta\lambda_{GPS} - \delta\lambda_{INS} \\ \delta h_{GPS} - \delta h_{INS} \end{bmatrix}$$

Since only position information is used to aid the INS system in an LC integration, the design matrix relating the error states to the measurement error is given by:

$$H = \begin{bmatrix} 1 & 0 & 0 & 0 & 0 & 0 & 0 & 0 & 0 \\ 0 & 1 & 0 & 0 & 0 & 0 & 0 & 0 & 0 \\ 0 & 0 & 1 & 0 & 0 & 0 & 0 & 0 & 0 \end{bmatrix}$$

Therefore, the measurement model can be expressed as:

$$\delta z = \begin{bmatrix} 1 & 0 & 0 & 0 & 0 & 0 & 0 & 0 & 0 \\ 0 & 1 & 0 & 0 & 0 & 0 & 0 & 0 & 0 \\ 0 & 0 & 1 & 0 & 0 & 0 & 0 & 0 & 0 \end{bmatrix} \begin{bmatrix} \delta\varphi \\ \delta\lambda \\ \delta h \\ \delta v^e \\ \delta v^n \\ \delta v^u \\ \delta A_z \\ \delta a_{od} \\ \delta b_z \end{bmatrix} + \eta$$

E. Extended Kalman Filter

There are many types of filters used to fuse INS and GPS solutions in order to produce an optimal estimation of the states of the system. The most common filters are KF and Particle Filter (PF) which are recursive Bayesian estimators. In this research, we have implemented a closed loop configuration of KF which is known as Extended Kalman Filter (EKF). The main advantage of PF over KF is that the system and measurement noise are not constrained to Gaussian distributions and hence PF could provide more accurate solutions. Moreover, the system and measurement models are not limited to linear systems just like the case in KF. However, the main advantage of KF over PF is the low complexity of the filter and the real time response. EKF is a closed loop implementation of the KF, where error states computed by KF are fed back to the INS mechanization stage to predict a more accurate INS solution and to keep the system model in the linearity region. Some critical parameters have to be initialized before the operation of KF. The initial system noise covariance matrix is denoted by Q_0 and the initial measurement covariance matrix is denoted by R_0. Moreover, the initial error states of the system are denoted by $\delta\hat{\mathbf{x}}_0$ and the initial state covariance matrix is denoted by P_0.

The KF algorithm consists of two main stages which are the prediction stage and the correction stage. In the prediction stage, the system transition matrix $\phi_{k,k-1}$ is used to predict the current error states at epoch k denoted by $\delta\hat{\mathbf{x}}_k^p$ from the previous corrected errors states denoted by $\delta\hat{\mathbf{x}}_{k-1}^c$. Moreover, the prediction stage includes computing the predicted state covariance matrix denoted by P_k^p using the knowledge of the previous corrected state covariance matrix denoted by P_{k-1}^c, the system transition matrix and the system noise covariance matrix. Equations 25 and 26 depict the prediction of the states and the states covariance matrix of the system.

$$\delta\hat{\mathbf{x}}_k^p = \phi_{k,k-1}\delta\hat{\mathbf{x}}_{k-1}^c \tag{25}$$

$$P_k^p = \phi_{k,k-1}P_{k-1}^c\phi_{k,k-1}^T + Q_0 \tag{26}$$

In this EKF, the system noise covariance matrix does not vary over time and is specific to the error characteristics of the inertial sensors. The next stage of the KF is the correction stage. In this stage, the KF gain denoted by K_k is computed as a function of the predicted state covariance matrix and the measurement noise covariance matrix which is denoted by R_k. The KF gain is computed using the following Equation:

$$K_k = P_k^p H_k^T \left\{ H_k P_k^p H_k^T + R_k \right\}^{-1} \tag{27}$$

The R_k is propagated from the LS estimator to the KF at each epoch and represents the confidence in the $\delta\varphi$, $\delta\lambda$ and δh. The next step in the correction stage is to calculate the corrected states. The innovation vector depicted in Equation 28 is a quantity describing the difference between the measured error states denoted by δz_k and the predicted error states. The corrected error states denoted by $\delta\hat{\mathbf{x}}_k^c$ are computed using Equation 29. When K_k approaches zero (measurement is unreliable), the corrected and predicted error states are equal. As the KF gain increases (measurement is reliable), a larger quantity of the innovation vector is used to correct the predicted error states. The final step of the KF correction stage is shown in Equation 30 and is used to compute the corrected state covariance matrix based on the calculated KF gain and the predicted state covariance matrix. The corrected states and the corrected states covariance matrix are propagated to the next epoch.

$$\upsilon_k = \delta z_k - H_k\delta\hat{\mathbf{x}}_k^p \tag{28}$$

$$\delta\hat{\mathbf{x}}_k^c = \delta\hat{\mathbf{x}}_k^p + K_k\upsilon_k \tag{29}$$

$$P_k^c = P_k^p + K_k H_k P_k^p \tag{30}$$

In an EKF, the state prediction step depicted in Equation 25 is not considered because of the closed loop implementation. In the closed loop implementation, the corrected error states are fed back to the INS mechanization stage and the previous error states are set to zero. Therefore, the predicted error states are always zero and the first step in the prediction stage is unnecessary.

IV. Experiments and Results

In order to test the proposed cooperative system, a target and an assisting vehicle are employed in a real road trajectory in Kingston, Ontario. In this section, we present the equipment used to conduct a real road trajectory in order to evaluate the proposed cooperative system. Secondly, the evaluation criteria which is used to test the performance of our system

TABLE II
IMU CHARACTERISTICS OF IMU-CPT [30] AND CROSSBOW IMU300CC [31]

Characteristics	IMU-CPT	Crossbow IMU300CC
Size	15.2x16.8x8.9 cm	7.62x9.53x8.13 cm
Gyro Technology	FOG	MEMS
Weight	2.36 Kg	0.59 Kg
Max Data-rate	100 Hz	200 Hz
Start-up Time	N/A	$<$1s
Accelerometer Characteristics		
Range	$\pm 10g$	$\pm 2g$
Bias	$\pm 50mg$	$<\pm 30mg$
Bias Stability	$\pm 0.75mg$	N/A
Scale Factor	4000 ppm	$<1\%$
Random Walk	N/A	$<0.15m/s/\sqrt{hr}$
Gyroscope Characteristics		
Range	$\pm 375^\circ/s$	$\pm 100^\circ/s$
Bias	$20^\circ/hr$	$<\pm 2^\circ/s$
Bias Stability	$\pm 1^\circ/hr$	N/A
Scale Factor	1500 ppm	$<1\%$
Random Walk	$<0.0667^\circ/\sqrt{hr}$	$<2.25^\circ/\sqrt{hr}$

is introduced. In addition, the experimental setup for the real road trajectory is described. Finally, the results are presented and analyzed.

A. Equipment

There are two IMUs used in this experiment, a high tactical grade IMU from Novatel called IMU-CPT and a MEMS-based IMU called Crossbow IMU300CC. High grade IMUs are not used in commercial land vehicle applications due to their high cost. However, here we use IMU-CPT to aid the GPS system in estimating the reference solution. On the other hand, MEMS-based IMUs can be used in commercial land vehicle applications because they are less expensive and light weight. The proposed system uses data from Crossbow IMU300CC. The characteristics of the high tactical grade and the MEMS-based IMUs are depicted in Table II. It is important to mention that the IMU-CPT employs a full IMU mechanization process by utilizing 3-axis accelerometers and 3-axis gyroscopes, however, the RISS mechanization used in this research only utilizes the vertical gyroscope and the two horizontal accelerometers from the MEMS-based IMU along with the wheel rotation sensor readings to compute the states of the target vehicle.

The RISS mechanization process requires information about the speed of the vehicle. This is acquired by using a speed logger. CarChip [32] is a data logger which was connected to the OBDII interface of the target vehicle. This data logger records the speed of the vehicle and saves it on a flash memory. The memory can be accessed offline through the CarChip software installed on a laptop. The logged speeds are then synchronized with the GPS time tag as a post-processing step.

There are two types of GNSS receivers used in our experiments, the NovAtel SPAN-SE reference system and the NovAtel ProPak-G2plus GPS receiver. The SPAN-SE unit integrates GNSS signals with the high tactical grade IMU-CPT in a tightly coupled KF using L1 and L2 signals. The SPAN-SE is installed inside the target vehicle with two antennas and the output from the SPAN-SE is used as a reference solution. The second type of receivers used is a GPS receiver (NovAtel ProPak-G2plus) capable of decoding only GPS signals.

The equipment installed on the target vehicle is:

1) Two L1 and L2 GNSS antennas (GPS-702-GG) offering combined GPS and GLONASS signal reception. Here, two antennas are used to aid SPAN-SE unit in accurately determining the heading of the target vehicle.
2) The SPAN-SE GNSS receiver which offers GPS standalone solution and an integrated IMU-CPT/GNSS solution.
3) A high tactical grade IMU called IMU-CPT offering full IMU 3D solution.
4) A Data logger (CarChip) that is connected to the OBDII interface collecting speed logs.

The equipment installed on the assisting vehicle are:

1) An L1 and L2 GNSS antenna (GPS-702-GG) offering combined GPS and GLONASS signal reception.
2) A NovAtel ProPak-G2plus GPS receiver. The pseudoranges from GLONASS satellites are not processed.

B. Evaluation Criteria

The purpose of this experiment is to investigate if the proposed cooperative 3D-RISS/GPS LC-EKF (CLC-EKF) is capable of outperforming the conventional non-cooperative 3D-RISS/GPS LC-EKF (NLC-EKF) during partial GPS outages in urban environments. If the target vehicle does not have an INS system installed, there will be no solution available during partial GPS outages. However, if a commercial INS system is installed, a solution is available but its accuracy degrades exponentially as the GPS outage duration prolongs. In order to evaluate the proposed cooperative system, we collect data from two vehicles in an open sky environment and then manually introduce GPS partial outages. The 2D RMS error of the position estimated by the CLC-EKF is compared to the 2D RMS error of the position estimated by the NLC-EKF. The 2D RMS value is computed using the following Equation:

$$RMS = \frac{\sum_{n=1}^{N} \sqrt{(\varphi_n - \hat{\varphi}_n)^2 + (\lambda_n - \hat{\lambda}_n)^2}}{N} \tag{31}$$

Where φ_n and λ_n are respectively the reference latitude and longitude of the target vehicle for the nth pseudorange samples. Moreover, $\hat{\varphi}_n$ and $\hat{\lambda}_n$ are respectively the estimated latitude and longitude using the positioning systems under evaluation (CLC-EKF or NLC-EKF). The number of available pseudorange samples are denoted by N. The second metric used to evaluate the proposed system is the Positioning Accuracy Gain (PAG) and is given by Equation 32. Where $RMS_{CLC-EKF}$ is the 2D RMS position error of the CLC-EKF system and $RMS_{NLC-EKF}$ is the 2D RMS position error of the NLC-EKF system. Finally, the third metric used to evaluate the performance of the proposed system is the maximum 2D position error.

$$PAG = \frac{RMS_{NLC-EKF} - RMS_{CLC-EKF}}{RMS_{NLC-EKF}} \times 100 \tag{32}$$

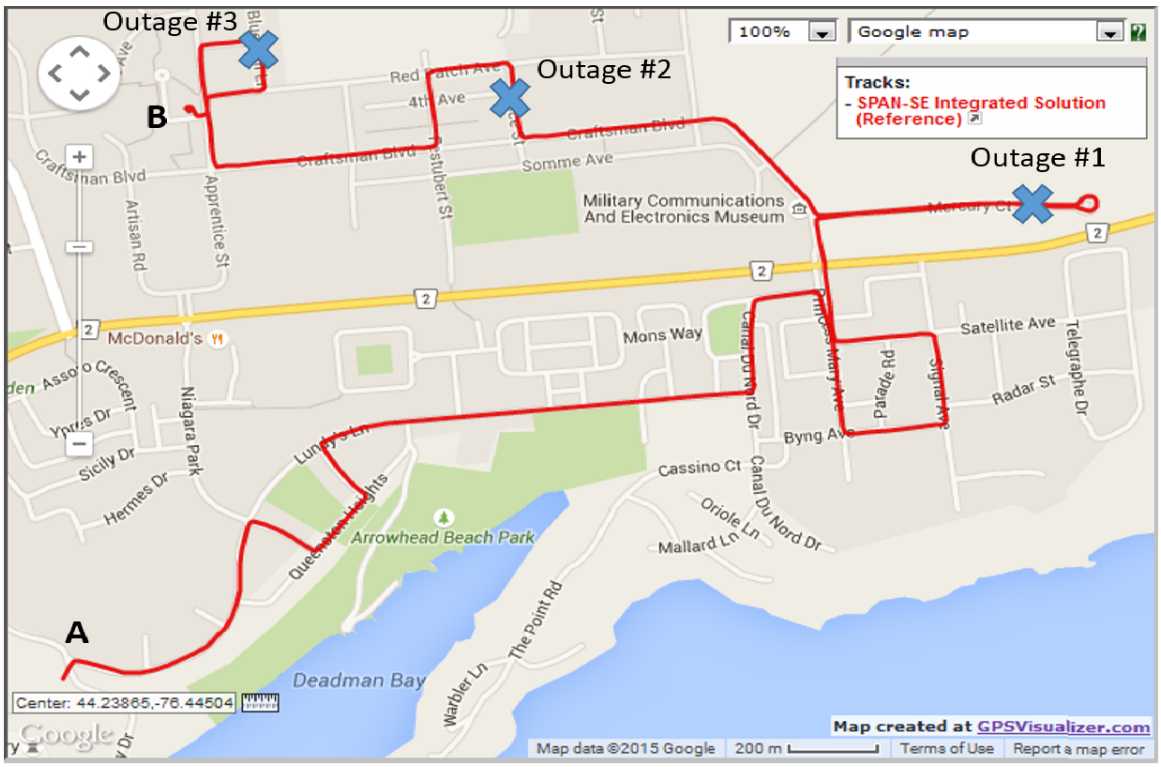

Fig. 3. Road trajectory estimated using NovAtel SPAN-SE unit.

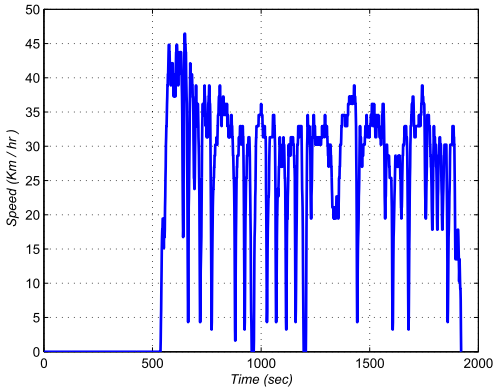

Fig. 4. Speed of the target vehicle for the road trajectory.

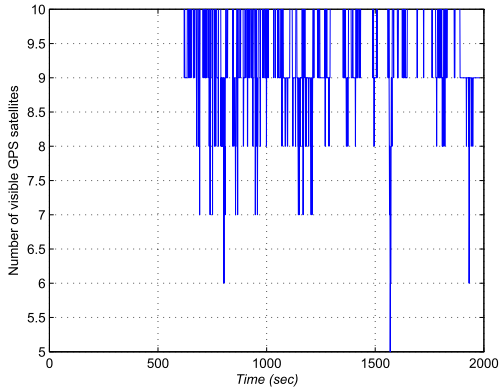

Fig. 5. Number of visible GPS satellites.

C. Experimental Setup

The road trajectory of the target vehicle and the assisting vehicle is shown in Figure 3. This trajectory is computed using the SPAN-SE unit installed on the target vehicle. On the map, points marked "A" and "B" are the start and end point of the trajectory respectively. Moreover, the blue crosses show the segments of the trajectory where partial GPS outage was introduced later in the offline phase. The speed of the target vehicle throughout the trajectory is shown in Figure 4. The average speed is 20.42 Km/hr, the maximum speed is 46.44 Km/hr and the speed standard deviation is 14.87 Km/hr. The average distance between the target and the assisting vehicle is 35 meters and the minimum distance is 15 meters. The trajectory was conducted in an open sky environment so we can easily block any visible satellite in the offline stage and test our system with different satellites' geometries relative to the position of the vehicles. The number of visible GPS satellites to the target vehicle is shown in Figure 5. In order to mimic the limited number of visible satellites in urban areas due to tall buildings, initially only four satellites were made visible to the target and the assisting vehicle in the outage segments of the trajectory. The number of common satellites is four and is denoted by CS. The four satellites with the highest elevation angles were used as the common visible satellites.

The next step is to reduce the number of common satellites by blocking one, two or three satellites from the four satellites which were initially visible to the target vehicle. Thus, mimicking the effect of vehicles in an urban area having with

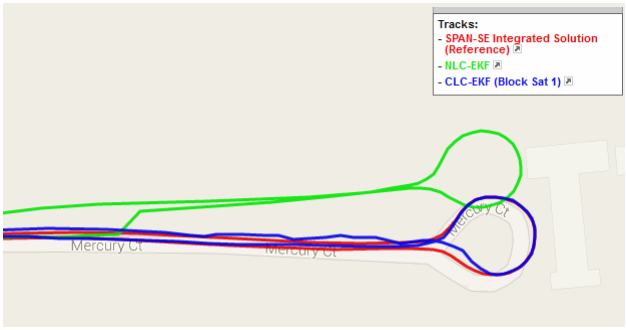

Fig. 6. Estimated trajectory using NLC-EKF and CLC-EKF compared to the reference solution for the first outage when the highest elevation satellite is blocked.

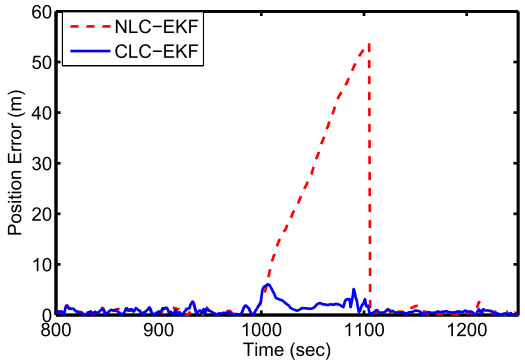

Fig. 7. Position error of NLC-EKF and CLC-EKF for the first outage when the highest elevation satellite is blocked.

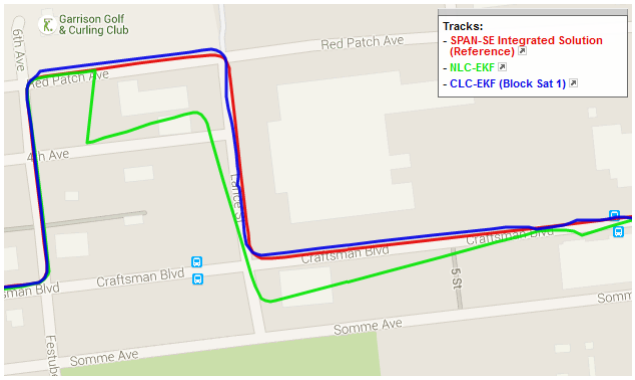

Fig. 8. Estimated trajectory using NLC-EKF and CLC-EKF compared to the reference solution for the second outage when the highest elevation satellite is blocked.

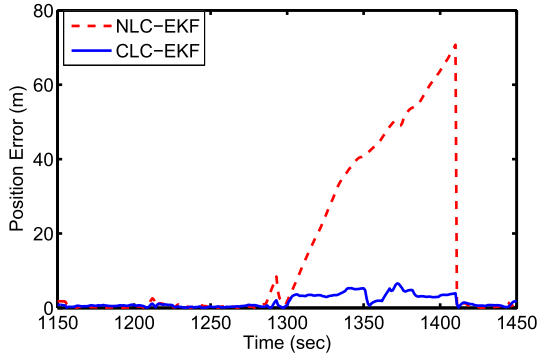

Fig. 9. Position error of NLC-EKF and CLC-EKF compared to the reference solution for the second outage when the highest elevation satellite is blocked.

different positioning resources. The number of visible satellites is still four for the assisting vehicle. This might occur for example when the assisting vehicle is capable of decoding GPS and GLONASS while the target vehicle decodes only GPS signals. Now the conventional 3D-RISS/GPS integration using LC-EKF will rely only on RISS solution (positioning accuracy degrades exponentially during the outage) since GPS is partially blocked from the target vehicle and the number of visible satellites is less than four. Here, we apply the proposed cooperative system which applies AA and consequently generates a number of ACPs that is equal to CS. The next step is to select the most accurate ACP using the ASODD selection criteria if CS is not equal one. The selected ACP or ACPs (depending on the number of blocked satellites) are then passed to the LS algorithm along with the measured pseudoranges to the visible satellites to compute the GPS position of the target vehicle. Finally, a LC-EKF is used to integrate the GPS solution with the 3D-RISS solution and a final estimate of the error states of the system are computed. These error states are used to correct the solution of the 3D-RISS system.

The duration of each of the three outage regions is 100 seconds. We know that the accuracy of the generated ACPs is a function of the satellite geometry relative to the target and assisting vehicle. In order to diversify the possible geometries and hence produce reliable results, the three outage regions were chosen such that a sharp change in the direction of the trajectory occurs during each outage segment. Moreover, another technique used to diversify the possible geometries is by blocking all possible combinations of visible satellites to the target vehicle and then averaging the horizontal RMS error.

D. Results

Figures 6, 8 and 10 depict the estimated trajectory on Google maps using the conventional NLC-EKF and the proposed CLC-EKF for the first, second and third outage segments respectively. Both NLC-EKF and CLC-EKF are compared to the reference solution from the SPAN-SE unit. The highest elevation satellite was blocked for a duration of 100 seconds. The number of common satellites between the target and the assisting vehicles was three and hence three ACPs were generated using AA. Subsequently, ASODD was applied and one ACP was selected and then used to compute the GPS position using LS algorithm. Finally, LC-EKF was applied to the RISS and the GPS position to produce the CLC-EKF solution. On the other hand, the NLC-EKF relied only on the 3D-RISS output since a minimum of 4 satellites is required to compute a GPS position.

Figures 7, 9 and 11 depict the 2D position error in meters using the conventional NLC-EKF and the proposed CLC-EKF for the first, second and third outage segments respectively. These errors are for the same simulation setup (blocking the highest elevation satellite) that was used to estimate the trajectories in Figures 6, 8 and 10. It is clear that the NLC-EKF position errors accumulate over time during the outage segments of the trajectory. On the other hand, the CLC-EKF position errors are not accumulative and are significantly better than the conventional NLC-EKF.

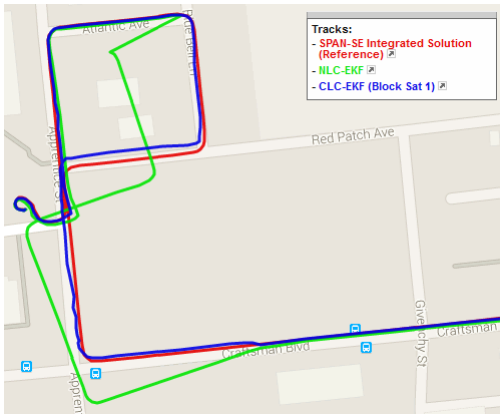

Fig. 10. Estimated trajectory using NLC-EKF and CLC-EKF compared to the reference solution for the third outage when the highest elevation satellite is blocked.

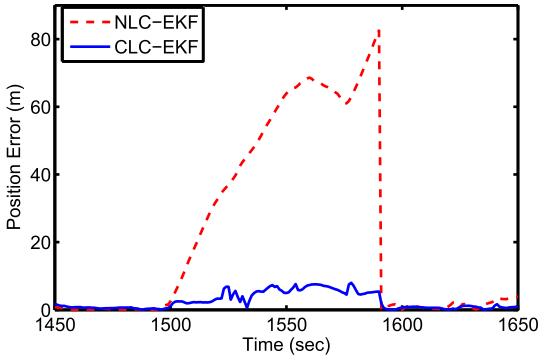

Fig. 11. Position error of NLC-EKF and CLC-EKF for the third outage when the highest elevation satellite is blocked.

TABLE III
OUTAGE # 1

No. of Blocked Satellites	NLC-EKF RMS (m)	NLC-EKF Max. Error (m)	CLC-EKF RMS (m)	CLC-EKF Max. Error (m)	PAG (%)
1	33	53.5	3.9	9.04	88.1
2	33	53.5	6.4	14.4	80.6
3	33	53.5	14.1	20	57.27

Tables V, IV and V shows the RMS and the maximum 2D position error for the estimated position using NLC-EKF and CLC-EKF for the first, second and third outage segments respectively. The RMS and maximum 2D position error is computed for different number of blocked satellites between the target and the assisting vehicle during the outage segments. The CLC-EKF was applied for one, two and three blocked satellites. For a specific number of blocked satellites, there are many combination of visible satellites. The 2D position error for each combination is different due to the sensitivity of the AA to satellite geometry relative to the position of both vehicles and also due to different accuracies of the measured pseudoranges by the target vehicle. In order to compute a realistic RMS error of the 2D position estimated by CLC-EKF, all possible combinations of satellites were considered in the RMS calculations for each number of blocked satellites setup. The RMS errors shown in Tables V, IV and V are a result of applying CLC-EKF to all possible satellite combinations for each number of blocked satellites.

TABLE IV
OUTAGE # 2

No. of Blocked Satellites	NLC-EKF RMS (m)	NLC-EKF Max. Error (m)	CLC-EKF RMS (m)	CLC-EKF Max. Error (m)	PAG (%)
1	38.27	68.74	4.4	10.2	88.5
2	38.27	68.74	7.3	17.7	80.92
3	38.27	68.74	15.5	25	59.5

TABLE V
OUTAGE # 3

No. of Blocked Satellites	NLC-EKF RMS (m)	NLC-EKF Max. Error (m)	CLC-EKF RMS (m)	CLC-EKF Max. Error (m)	PAG (%)
1	42.7	80.5	5	13.3	88.29
2	42.7	80.5	8.1	20	81
3	42.7	80.5	16	42	62.52

First of all, we observe that the solution of the CLC-EKF is always better than the NLC-EKF in terms of the 2D RMS position error and the maximum position error regardless of the number of blocked satellites for all three outage segments. Moreover, as the number of blocked satellites decrease, the gain of the proposed cooperative system increases compared to the conventional non-cooperative system. The 2D RMS position error and the maximum error of the NLC-EKF is the higher for third outage segment compared to the first and the second outage segment. This error also affects the proposed system due to the uncompensated gyroscope errors. Correcting the gyroscope angular rate errors should result in lower heading errors and therefore lower 2D RMS position errors for the NLC-EKF and the CLC-EKF systems. Using the proposed cooperative system (CLC-EKF) results in higher positioning accuracy during partial GPS outages. The PAG gain is around 88%, 80% and 60% when the number of blocked satellites is one, two and three respectively.

V. CONCLUSION

ITS applications demand specific positioning availability and accuracy requirements. In urban areas, GNSS signals are hindered due to tall buildings, multipath effect, jamming and limited GNSS channels per receiver; this leads to limited positioning availability and accuracy. This paper proposed the CLC-EKF system which integrates RISS and GPS using EKF and assists GPS during partial outages. The proposed system is implemented and tested using road trajectories and compared to the conventional NLC-EKF system. The proposed CLC-EKF outperforms the conventional NLC-EKF system in terms of position RMS error and the maximum position error. Specifically, the PAG gain was around 88%, 80% and 60% when the number of blocked satellites during partial GPS outages is one, two and three respectively.

REFERENCES

[1] N. Alam, "Vehicular positioning enhancement using DSRC," Ph.D. dissertation, School Surveying Spatial Inf. Syst., Univ. New South Wales, Sydney, NSW, Australia, 2012.

[2] N. Alam, A. T. Balaei, and A. G. Dempster, "Range and range-rate measurements using DSRC: Facts and challenges," in *Proc. Int. Global Navigat. Satell. Syst. Soc. (IGNSS Symp.)*, Surfers Paradise, 2009, pp. 1–14.

[3] A. J. Weiss, "On the accuracy of a cellular location system based on RSS measurements," *IEEE Trans. Veh. Technol.*, vol. 52, no. 6, pp. 1508–1518, Nov. 2003.
[4] G. Mao, B. D. O. Anderson, and B. Fidan, "Online calibration of path loss exponent in wireless sensor networks," in *Proc. IEEE Global Telecommun. Conf. (GLOBECOM)*, San Francisco, CA, USA, Nov./Dec. 2006, pp. 1–6.
[5] G. Mao, B. D. O. Anderson, and B. Fidan, "Path loss exponent estimation for wireless sensor network localization," *Comput. Netw.*, vol. 51, no. 10, pp. 2467–2483, Jul. 2007.
[6] X. Li, "RSS-based location estimation with unknown pathloss model," *IEEE Trans. Wireless Commun.*, vol. 5, no. 12, pp. 3626–3633, Jul. 2006.
[7] N. Drawil and O. Basir, "Vehicular collaborative technique for location estimate correction," in *Proc. IEEE 68th Veh. Technol. Conf.*, Calgary, BC, Canada, Sep. 2008, pp. 1–5.
[8] N. Drawil and O. Basir, "Toward increasing the localization accuracy of vehicles in VANET," in *Proc. IEEE Int. Conf. Veh. Electron. Safety*, Pune, India, Nov. 2009, pp. 13–18.
[9] D. Zhou and T. H. Lai, "An accurate and scalable clock synchronization protocol for IEEE 802.11-based multihop ad hoc networks," *IEEE Trans. Parallel Distrib. Syst.*, vol. 18, no. 12, pp. 1797–1808, Dec. 2007.
[10] D.-H. Shin and T.-K. Sung, "Comparisons of error characteristics between TOA and TDOA positioning," *IEEE Trans. Aerosp. Electron. Syst.*, vol. 38, no. 1, pp. 307–311, Jan. 2002.
[11] A. U. Peker, T. Acarman, Ç. Yaman, and E. Yüksel, "Vehicle localization enhancement with VANETs," in *Proc. IEEE Intell. Vehicles Symp.*, Dearborn, MI, USA, Jun. 2014, pp. 661–666.
[12] N. A. Alsindi, B. Alavi, and K. Pahlavan, "Measurement and modeling of ultrawideband TOA-based ranging in indoor multipath environments," *IEEE Trans. Veh. Technol.*, vol. 58, no. 3, pp. 1046–1058, Mar. 2009.
[13] A. Y.-Z. Xu, E. K. S. Au, A. K.-S. Wong, and Q. Wang, "A novel threshold-based coherent TOA estimation for IR-UWB systems," *IEEE Trans. Veh. Technol.*, vol. 58, no. 8, pp. 4675–4681, Oct. 2009.
[14] C. Falsi, D. Dardari, L. Mucchi, and M. Z. Win, "Time of arrival estimation for UWB localizers in realistic environments," *EURASIP J. Appl. Signal Process.*, vol. 2006, Jul. 2006, Art. no. 032082, doi: 10.1155/ASP/2006/32082.
[15] X. Wang, Z. Wang, and B. O'Dea, "A TOA-based location algorithm reducing the errors due to non-line-of-sight (NLOS) propagation," *IEEE Trans. Veh. Technol.*, vol. 52, no. 1, pp. 112–116, Jan. 2003.
[16] N. Alam, A. T. Balaei, and A. G. Dempster, "An instantaneous lane-level positioning using DSRC carrier frequency offset," *IEEE Trans. Intell. Transp. Syst.*, vol. 13, no. 4, pp. 1566–1575, Dec. 2012.
[17] N. Alam, A. T. Balaei, and A. G. Dempster, "A DSRC-based traffic flow monitoring and lane detection system," in *Proc. IEEE 73rd Veh. Technol. Conf.*, Budapest, Hungary, May 2011, pp. 1–5.
[18] N. Alam, "Three dimensional positioning with two GNSS satellites and DSRC for vehicles in urban canyons," presented at the 24th Int. Tech. Meeting Satell. Division Inst. Navigat., Portland, OR, USA, 2011, pp. 3975–3983.
[19] E. Richter, M. Obst, R. Schubert, and G. Wanielik, "Cooperative relative localization using vehicle-to-vehicle communications," in *Proc. 12th Int. Conf. Inf. Fusion*, Seattle, WA, USA, Jul. 2009, pp. 126–131.
[20] N. Alam, A. Tabatabaei Balaei, and A. G. Dempster, "A DSRC Doppler-based cooperative positioning enhancement for vehicular networks with GPS availability," *IEEE Trans. Veh. Technol.*, vol. 60, no. 9, pp. 4462–4470, Nov. 2011.
[21] N. Alam, A. T. Balaei, and A. G. Dempster, "Relative positioning enhancement in VANETs: A tight integration approach," *IEEE Trans. Intell. Transp. Syst.*, vol. 14, no. 1, pp. 47–55, Mar. 2013.
[22] K. Liu, H. B. Lim, E. Frazzoli, J. Houling, and V. C. S. Lee, "Improving positioning accuracy using GPS pseudorange measurements for cooperative vehicular localization," *IEEE Trans. Veh. Technol.*, vol. 63, no. 6, pp. 2544–2556, Jul. 2014.
[23] A. Mahmoud, "Non-range based cooperative localization for VANETs in urban environments," M.S. thesis, Dept. Elect. Comput. Eng., Queen's Univ., Kingston, ON, Canada, 2015.
[24] A. Mahmoud, A. Noureldin, and H. S. Hassanein, "VANETs positioning in urban environments: A novel cooperative approach," in *Proc. IEEE 82nd Veh. Technol. Conf.*, Boston, MA, USA, Sep. 2015, pp. 1–7.
[25] A. Mahmoud, A. Noureldin, and H. S. Hassanein, "Distributed vehicle selection for non-range based cooperative positioning in urban environments," in *Proc. IEEE Int. Conf. Commun.*, Kuala Lumpur, Malaysia, May 2016, pp. 1–6.
[26] J. Georgy, A. Noureldin, M. J. Korenberg, and M. M. Bayoumi, "Low-cost three-dimensional navigation solution for RISS/GPS integration using mixture particle filter," *IEEE Trans. Veh. Technol*, vol. 59, no. 2, pp. 599–615, Feb. 2010.
[27] U. Iqbal, F. Okou, and A. Noureldin, "An integrated reduced inertial sensor system-RISS/GPS for land vehicle," in *Proc. IEEE/ION Position, Location Navigat. Symp.*, Monterey, CA, USA, May 2008, pp. 1014–1021.
[28] J. Georgy, A. Noureldin, M. J. Korenberg, and M. M. Bayoumi, "Modeling the stochastic drift of a MEMS-based gyroscope in gyro/odometer/GPS integrated navigation," *IEEE Trans. Intell. Transp. Syst.*, vol. 11, no. 4, pp. 856–872, Dec. 2010.
[29] A. Noureldin, T. B. Karamat, and J. Georgy, *Fundamentals of Inertial Navigation, Satellite-Based Positioning and Their Integration*. Heidelberg, Germany: Springer, 2013.
[30] *NovAtel SPAN-CPT User Manual OM-20000122*, NovAtel, Calgary, AB, Canada, 2014.
[31] *IMU Users Manual-Models IMU300CC, IMU400CC, IMU400CD*, Crossbow Technol., Milpitas, CA, USA, 2007.
[32] *CarChip OBDII-Based Vehicle Data Logger and Software*, Davis Instrum. Corp., Hayward, CA, USA, 2012.

Anas Mahmoud received the B.Sc. degree in information engineering and technology (major: telecommunications) from German University in Cairo, New Cairo, Egypt, in 2012, the M.Sc. degree in electrical and computer engineering from Queen's University, Kingston, ON, Canada, in 2015, and the master's degree in computer science from the Georgia Tech Institute of Technology. He was a GNSS Algorithm Developer of the Research and Development GNSS Team, Esterline CMC Electronics. He is currently a Staff Algorithm Designer with the Navigation Research and Development Team, TDK Corporation. He is also a part-time Student with the Georgia Tech Institute of Technology. He has filed four U.S. patents in the field of path-planning and sensor fusion for navigation.

Aboelmagd Noureldin (S'98–M'02–SM'08) received the B.Sc. degree in electrical engineering and the M.Sc. degree in engineering physics from Cairo University, Giza, Egypt, in 1993 and 1997, respectively, and the Ph.D. degree in electrical and computer engineering from the University of Calgary, Calgary, AB, Canada, in 2002. He is currently a Professor with the Department of Electrical and Computer Engineering, Royal Military College of Canada (RMCC), Kingston, ON, Canada. He is also the Founder and the Director of the Navigation and Instrumentation Research Group, RMCC. He has authored more than 200 papers published in journals and conference proceedings. His research work led to several patents in the areas of position, location, and navigation. His research interests include GPS, wireless location and navigation, indoor positioning, and multisensor fusion.

Hossam S. Hassanein (S'86–M'90–SM'05–F'16) is a leading authority in the areas of broadband, wireless, and mobile networks architecture, protocols, control, and performance evaluation. He is currently the Founder and the Director of the Telecommunications Research Laboratory, School of Computing, Queen's University, with extensive international academic and industrial collaborations. His record spans more than 500 publications in journals, conferences, and book chapters, in addition to numerous keynotes and plenary talks in flagship venues. He received several recognitions and the best paper awards at top international conferences. He is the former Chair of the IEEE Communication Society Technical Committee on Ad Hoc and Sensor Networks. He is a Distinguished Speaker of the IEEE Communications Society (Distinguished Lecturer from 2008 to 2010).